

# Soft Matter

Accepted Manuscript



This is an *Accepted Manuscript*, which has been through the Royal Society of Chemistry peer review process and has been accepted for publication.

*Accepted Manuscripts* are published online shortly after acceptance, before technical editing, formatting and proof reading. Using this free service, authors can make their results available to the community, in citable form, before we publish the edited article. We will replace this *Accepted Manuscript* with the edited and formatted *Advance Article* as soon as it is available.

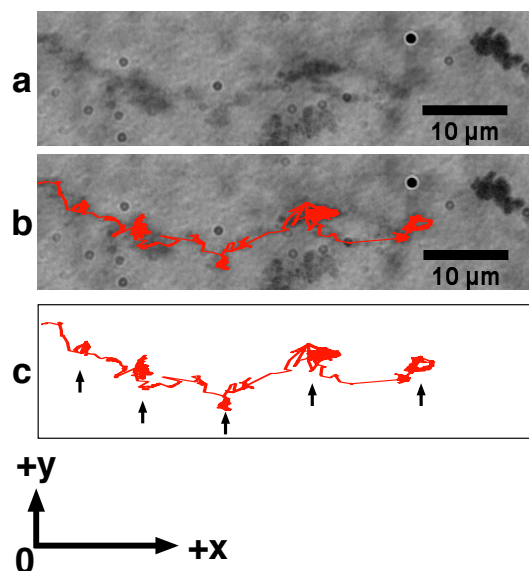
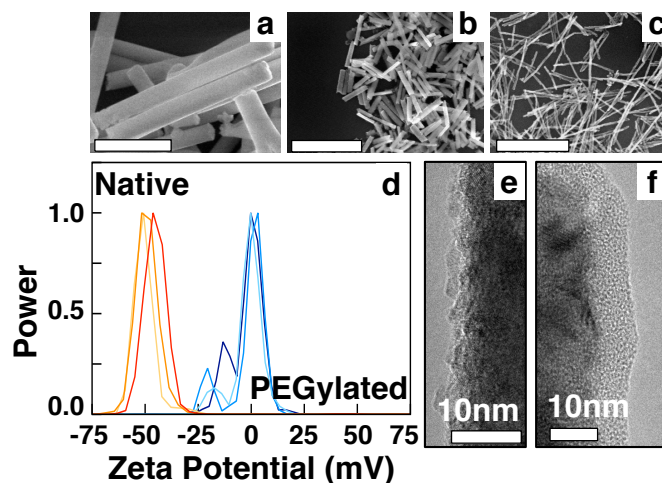
You can find more information about *Accepted Manuscripts* in the [Information for Authors](#).

Please note that technical editing may introduce minor changes to the text and/or graphics, which may alter content. The journal's standard [Terms & Conditions](#) and the [Ethical guidelines](#) still apply. In no event shall the Royal Society of Chemistry be held responsible for any errors or omissions in this *Accepted Manuscript* or any consequences arising from the use of any information it contains.

## Single Particle Tracking Reveals Biphasic Transport During Nanorod Magnetophoresis Through Extracellular Matrix

L.O. Mair, R. Superfine

Magnetic drug targeting has been proposed as a means of efficiently targeting drugs to tumors. However, the extracellular matrix (ECM) remains a significant barrier to long-range magnetophoretic transport through the tumor volume. While ensemble measurements of nanoparticle magnetophoresis have been reported, a single particle level understanding of magnetophoretic transport remains at large. We quantify nanorod magnetophoresis through ECM based on single particle observations. We find that smaller diameter particles achieve larger velocities through ECM despite experiencing smaller magnetic forces. Additionally, two interesting dynamics are elucidated. First, 18 nm diameter nanorods experience bimodal stick-slip motion through ECM during static field magnetophoresis, while similar bimodal transport is not observed for 55 nm nor 200 nm diameter nanorods. Second, smaller particles experience larger deviations in their orientation angle with respect to the magnetic field. This work elucidates important dynamics of nanoparticle transport through complex, porous biomaterials that may go unnoticed during ensemble measurements.



## ARTICLE

# Single Particle Tracking Reveals Biphasic Transport During Nanorod Magnetophoresis Through Extracellular Matrix

Cite this: DOI: 10.1039/x0xx00000x

L.O. Mair<sup>a,c,\*</sup> and R. Superfine<sup>b</sup>

Received 00th March 2014,  
Accepted 00th -----

DOI: 10.1039/x0xx00000x

[www.rsc.org/](http://www.rsc.org/)

Magnetic drug targeting has been proposed as a means of efficiently targeting drugs to tumors. However, the extracellular matrix (ECM) remains a significant barrier to long-range magnetophoretic transport through the tumor volume. While ensemble measurements of nanoparticle magnetophoresis have been reported, a single particle level understanding of magnetophoretic transport remains at large. We quantify nanorod magnetophoresis through ECM based on single particle observations. We find that smaller diameter particles achieve larger velocities through ECM despite experiencing smaller magnetic forces. Additionally, two interesting dynamics are elucidated. First, 18 nm diameter nanorods experience bimodal stick-slip motion through ECM during static field magnetophoresis, while similar bimodal transport is not observed for 55 nm nor 200 nm diameter nanorods. Second, smaller particles experience larger deviations in their orientation angle with respect to the magnetic field. This work elucidates important dynamics of nanoparticle transport through complex, porous biomaterials that may go unnoticed during ensemble measurements.

## 1. Introduction

Nanoparticle (NP) delivery to solid tumors involves a series of mass transport processes through complexly structured biopolymer networks. Many of these biomaterials serve to inhibit effective, long-range distribution of NPs throughout the tumor volume. As such, one goal of the emerging field of transport oncophysics is to improve our understanding of the various mass transport processes involved in effective drug delivery to and within tumors<sup>1,2</sup>. Several review articles discuss the difficulties of intratumoral drug delivery<sup>3-6</sup>. While many studies have been performed quantifying magnetic particle transport through synthetic<sup>7-11</sup> and biological<sup>12-15</sup> polymer systems, fundamental questions about the dynamics of nanoparticle transport through biopolymer systems remain unanswered<sup>16</sup>. How do particles move in the complex environments of tissues? When pulled by a static magnetic gradient, do they experience constant velocity motion? A better understanding of how nanoparticles move during magnetic guidance through biological materials is critical for predicting how they will behave when implemented *in vivo*<sup>16</sup>.

From the blood stream there are three specific barriers which a NP-based therapeutic must traverse before reaching the interior of a tumor cell. After being administered, the NP must first cross the blood vessel wall to move from the blood stream into the tumor cell environment. Interestingly, angiogenesis results in tumor blood vessels which are comparatively leaky, with pores ranging from hundreds of nanometers to a few microns in diameter<sup>17</sup>. This is large compared with healthy blood vessels, which typically have pores only tens of nanometers in diameter. Following transport through the blood vessel wall, NPs must transit through the densely woven mesh of the extracellular matrix. The third physical barrier is, generally, the cell membrane. Each of these barriers pose specific difficulties

for particles, as each biopolymer material has its own protein constituents and structure, from which follows its membrane function. Each inhibitory barrier has its own exclusionary guidelines with respect to nanoparticle size and surface chemistry (although generally, particles with very little surface charge pass most efficiently through these protein-rich environments<sup>18-20</sup>).

Magnetic nanoparticles (MNPs) have been implemented in drug and gene delivery<sup>21,22</sup> for tumors<sup>23</sup> as well as tissue generation<sup>24</sup>. Specifically, magnetic drug targeting (MDT) seeks to magnetically capture drug-loaded nanoparticles at a specified tumor location, continually applying magnetic fields at the disease site so as to guide NPs to, and increase NP accumulation at, the relevant site, thereby increasing the local concentration of drug payload and minimizing the systemic drug dose<sup>25</sup>. Measuring magnetically induced nanoparticle transport through various materials informs our understanding of the transport dynamics at work and several studies have provided useful data quantifying ensemble transport of magnetic nanoparticles through various synthetic and biological polymer systems<sup>7,9-14</sup>. Ensemble measurements have elucidated transport kinetics of particles en masse, however our understanding of how individual particles translate through the complex protein meshwork of the ECM during magnetophoresis is incomplete. Cribb et al. performed quantitative assessments of single particle magnetophoretic transport through solutions of entangled DNA<sup>15</sup> and observed constant velocity motion for magnetic beads and rods moving through viscoelastic, partially entangled DNA solutions. However, DNA solutions are notably different from the extracellular matrix in fiber type, fiber dimensions, fiber connectivity, pore dimensions, and matrix homogeneity.

The ECM is composed primarily of collagen, laminin, and

glycosaminoglycans (GAGs), each contributing to the physical and chemical complexity of the matrix and the difficulty nanoparticles experience in traveling through the material. Collagen and laminin are fiber-forming proteins and compose the structural meshwork of the ECM<sup>26–28</sup>. GAGs are typically attached to the collagen-laminin latticework of the matrix<sup>29</sup>. Transport through the ECM is further complicated by the fact that these components organize themselves into a matrix that typically has pores ranging from 25 nm to 2  $\mu$ m in diameter, as demonstrated by the SEM micrographs of Matrigel shown in Fig. 1.

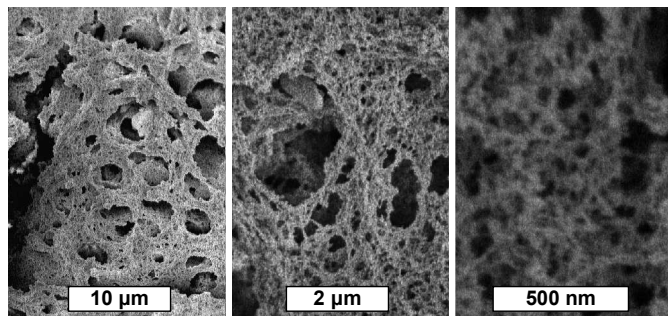


Figure 1: Scanning electron micrographs of prepared Matrigel.

Pore size polydispersity is a crucial component in gaining a complete and accurate understanding of MNP transport through the ECM. This matrix feature is not well-replicated by gels of synthetic polymers because (1) synthetic polymer gels typically do not contain the multidimensional fiber-like structures exhibited by collagen and laminin, and (2) synthetic polymer gels tend to organize more homogeneously and have lower pore size polydispersity. Indeed, it has been suggested that large pore size heterogeneity combined with the inherent and significant biological polymer stiffness found in mucus gels play a role in suppressing particle transport through mucus; Kirch et al. discovered that particle magnetophoresis was inhibited more by mucus than by hydroxyethylcellulose gels, despite these gels having higher viscosities and smaller pore dimensions<sup>30</sup>.

In addition to having a highly heterogeneous pore size, the ECM also functions as a charge-selective filter, effectively trapping particles carrying significant surface charges<sup>19,31</sup>. Thus, researchers seeking to achieve long-range nanoparticle transport through the tumor ECM typically implement a surface coating of polyethylene-glycol in order to mitigate surface charges on uncoated NPs. The need to mediate surface charge interactions between particles and their surrounding biopolymer matrix is another requirement which differentiates transport experiments performed in synthetic and biological polymer matrices.

## 2. Experimental Methods

We use template-guided electrodeposition to grow nickel nanorods in a custom electrodeposition cell. Standard three electrode deposition with a Pt auxiliary electrode, a Ag/AgCl double barrel reference electrode, and the thermally evaporated (Ag) template backing operating as the working electrode. Deposition is performed into the pores of Whatman Anodisc 13 anodized aluminum oxide (AAO) templates (200 nm diameter rods) or Synkera Inc. AAO templates (18 and 55 nm diameter rods). Following deposition we etch the Ag working electrode in 50% v/v nitric acid, then release the Ni nanorods by etching the AAO template in 0.5 M sodium hydroxide. Fabrication methods have been thoroughly documented in the literature<sup>32–34</sup>.

Proteins readily adsorb onto metal and metal oxide surfaces. Consequently, the particle surface plays a significant role in

determining a particle's ability to avoid motion-inhibiting interactions with the matrix and move through a dense network of biopolymers<sup>18,35–37</sup>. Overall particle behaviour in a protein network is therefore a consequence of composite factors, including steric, hydrodynamic, and chemical interactions. While particles may be small enough to move through the pores of a given protein mesh based exclusively on size, chemical interactions between the mesh proteins and the particle surface can induce non-specific binding, rendering the particle immobile. The metal oxide surfaces of the nanorods are natively covered with a hydroxyl layer. We modify the surfaces of all nanorods used in these experiments with methoxy-PEG-silane (1 kDa) according to the method demonstrated by Zhang et al.<sup>38</sup>, minimizing the zeta potential of all particles used in magnetophoresis experiments.

Following PEGylation, we concentrate nanorods and chill solutions to 4 °C. We then cold-pipette 1% v/v nanorod solution into Matrigel (chilled to 4 °C) and gently mix. Matrigel is an extracellular matrix composed primarily of collagen IV, laminin, and heparan sulfate proteoglycans isolated from the Engelbreth-Holm-Swarm (EHS) murine sarcoma. It is an accessible, purified, and readily available material for ECM-specific transport studies<sup>39</sup>. For these experiments, we store Matrigel at -30 °C until ready for use, then thaw it at 4 °C prior to mixing with nanorods. We store all pipettes, glass slides, and cover slips at 4 °C until use. After combining nanorods and Matrigel, we deposit a 7.5  $\mu$ l volume onto a #0 glass cover slip, sealing the volume with a 120  $\mu$ m thick polymer spacer (product #654008, Grace Bio-Labs) and another cover slip. Following sealing we incubate the sample at 37 °C for 1 hour in a humidity controlled incubator.

After incubation we place the sample on a microscope for brightfield transmitted light microscopy using a 100x dry objective (Fig. 2a). We use a Pulnix PTM-6710CL camera and custom software to collect video at 1 frame per second for tens of minutes; we use Video Spot Tracker software<sup>40</sup> (cismm.org) for tracking particles.

Magnetophoresis is performed in the static magnetic field of a calibrated cylindrical NdFeB permanent magnet (K&J Magnetics). The magnet and sample are aligned using a custom 3D printed polymer sample holder designed to center the focal plane of the sample with the center of the permanent magnet (Fig 2b). We calibrate the magnetic field using an F.W. Bell magnetometer at 250  $\mu$ m increments, from 18 mm to 80 mm away from the magnet face (Fig. 2c).

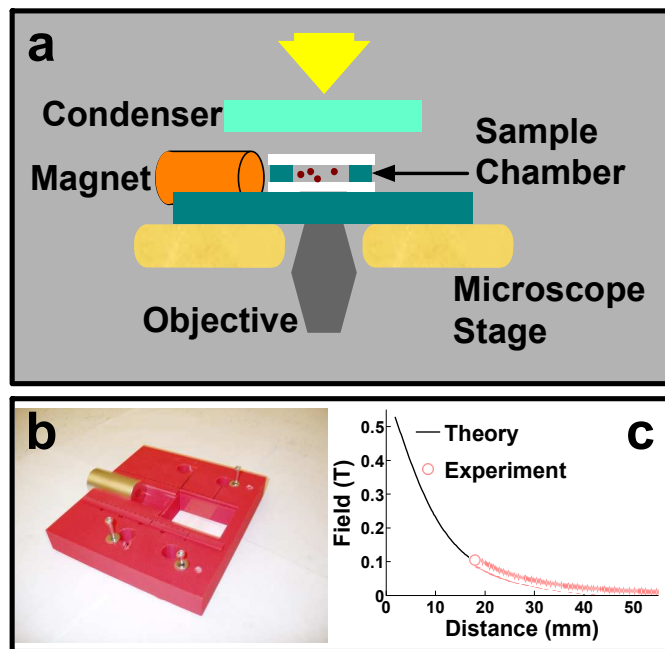


Figure 2: (a) Experimental setup. (b) Custom 3D printed microscope stage attachment for calibrated magnetophoresis experiments. (c) Experimental measurements of magnetic field (red circles) as a function of distance from the face of the magnet (measurements collected at 0.25 mm increments). The theoretical field and distance relationship based on Eq. 1 is shown (black line).

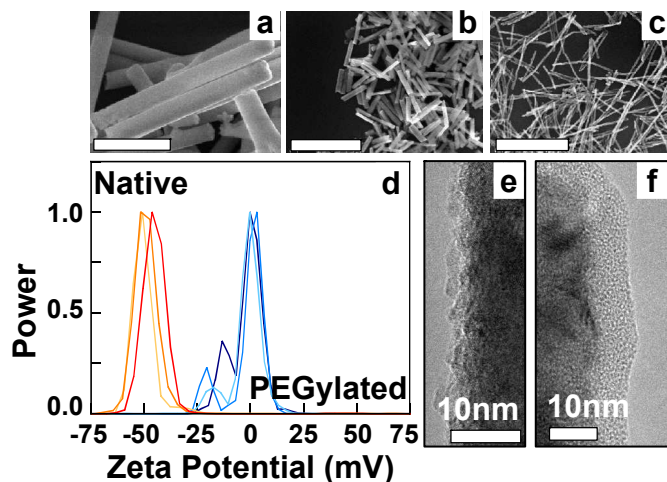


Figure 3: Scanning electron micrographs of nickel nanorods with nominal diameters of (a) 200 nm, (b) 55 nm, and (c) 18 nm. Scale bars in (a) – (c) are 1  $\mu\text{m}$ . Zeta potential measurements of rods reveal drastic differences before and after PEGylation (d). TEM images reveal the rough native oxide surface (e) and the smooth, functionalized PEG surface (f).

### 3. Results and Discussion

We prepare nickel nanorods of varying diameters using the method of template guided electrodeposition<sup>34</sup>. Scanning electron micrographs of as prepared rods are shown in Fig. 3a–c. We functionalize all nanorod surfaces with 1 kDa polyethylene glycol. Zeta potential measurements indicate that uncoated particles have an

average zeta potential of -46 mV, while PEGylated nanorods have an average of -3 mV (Fig. 3d). TEM images confirm this surface coating, showing the highly heterogeneous contrast and rough surface indicative of a native oxide and the more uniform contrast of the polymer coating (Fig. 3e and 3f). In assessing nanorod size and magnetophoretic force we use the as prepared diameters of the rods.

Using transmitted light microscopy, we observe and quantify single particle transport through Matrigel in vitro for various nanorod sizes. While nanorod diameters are below the diffraction limit, rod lengths are not. The lengths of the rods makes visualization possible without the need for fluorescence labeling or localization via plasmonic response<sup>41</sup>. For magnetophoretic transport through a homogenous Newtonian fluid the relevant forces acting on the magnetic particle are composed exclusively of the magnetic force applied by the permanent magnet and drag force of the surrounding fluid. Single particle magnetophoresis through water has been previously demonstrated for quantifying particle magnetic properties<sup>42</sup> and demonstrating the role diffusion plays in transport for a variety of nanovectors<sup>43</sup>. Experiments in Newtonian liquids make use of the equivalency  $F_{\text{drag}} = F_{\text{magnet}} = -\beta\eta v$ , where  $\beta$  is the particle geometry coefficient,  $\eta$  is the solution viscosity, and  $v$  is the particle velocity. As such, experiments in Newtonian solution can obtain  $F_{\text{magnet}}$  based on particle velocity, solution viscosity, and particle shape and size. In a gel network composed of connected fibrous proteins, the particles experience the additional steric force ( $F_{\text{steric}}$ ) imposed by the matrix fibers. Due to the immobile meshwork structure of the ECM, the sizes of the protein bundles involved, the sizes of the nanorods being pulled, and the innate heterogeneity of pores in the ECM, the requirements for implementing Stokes Law are not met. Thus, it cannot be used to fully describe nanorod magnetophoresis through the ECM. Later we will validate this via direct observation of particles experiencing large, inhibitory steric forces.

Because these experiments involve complex fibrous polymer systems, we take an analytical approach to calculating the magnetic force  $F_{\text{magnet}}$ , using the magnetic properties of the nanorods and the applied field and field gradient to determine  $F_{\text{magnet}}$ . We then use  $F_{\text{magnet}}$  and the observed nanorod velocities to assess the apparent viscosity  $\eta_{\text{apparent}}$  that is experienced by a nanorod in ECM. This apparent viscosity is a composite of both the drag force  $F_{\text{drag}}$  imposed by the liquid phase of the ECM, and the steric force  $F_{\text{steric}}$  imposed by the matrix. Importantly, because steric forces play a major role in inhibiting particle motion, the apparent viscosity  $\eta_{\text{apparent}}$  is expected to depend strongly, and nonlinearly, on particle diameter.

From previous work<sup>15</sup>, the magnetic force applied to a prolate ellipsoid can be calculated based on particle volume ( $V_c$  for a prolate ellipsoid), permeability ( $\mu_0$  for free space,  $\mu_r$  for the material of interest), and the magnetic field and field gradient present ( $B$  and  $\nabla B$ ). For our cylindrical nickel nanorods we use a prolate spheroid approximation, yielding  $F_{\text{magnet}} = [(u_r - 1)/2\mu_0] \cdot V_c \cdot B \nabla B$ , where  $V_c$  is the cylinder's volume<sup>44</sup>. Based on this relationship we calculate the forces on a nanorod of a given dimension. At the center of the magnet (along the magnet axis) the field of a cylindrical magnet  $B_m(z)$  is

$$B_m(z) = \frac{\mu_0 M_0}{2} \left[ \frac{L_m - z}{\sqrt{R_m^2 + (z - L_m)^2}} + \frac{z}{\sqrt{R_m^2 + z^2}} \right]$$

where  $\mu_0$  is the permeability of free space,  $M_0$  is the magnetic saturation of the magnet,  $L_m$  is one half the length of the magnet,  $R_m$  is the magnet radius, and  $z$  is the distance from the magnet center<sup>15</sup>. This relation is confirmed by our magnetic field measurements (Fig. 2c) and is useful in calculating the field and field gradient

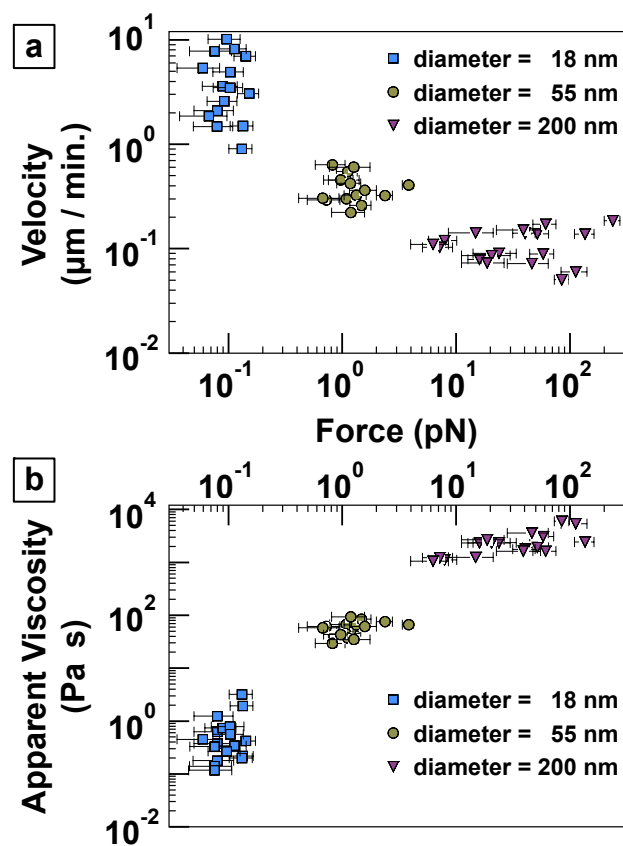


Figure 4: (a) demonstrates the discrepancy between  $F_{\text{magnet}}$  and velocity. Interestingly, data points for 18 nm diameter rods show relatively large variation in average velocity. Video analysis clearly indicates that long residence times exist for 18 nm diameter nanorods. The variation in velocity for both 55 nm and 200 nm rods is considerably smaller because of their unanimous steric hindrance: due to their larger diameters, all 55 nm and 200 nm diameter rods experienced significant steric hindrance at all times (as opposed to intermittent steric hindrance experienced by 18 nm diameter rods). (b) Treating Matrigel as a Newtonian material, the nanorod velocity as a function of diameter can be used to understand the particle's viscosity perspective as it travels, averaged over long travel times (minutes). Force distributions are considerably larger for 200 nm diameter rods due to significantly larger variation in nanorod lengths.

experienced by the nanorod: by analytically calculating the force on a rod of known dimensions we compare how this force scales with rod length for a given rod radius and can do so without using hydrodynamic drag equations to calculate the applied force. From this we obtain the force on the particle given any surrounding material environment. Additionally, we can compare these force expectations with experimental results for how the application of force on variously sized rods impacts nanorod transport. This relationship is confirmed by our field measurements (Fig. 2c).

Using the known rod diameters and measuring the lengths of individual rods undergoing magnetophoresis, we calculate nanorod volume and expected  $F_{\text{magnet}}$ . We plot these calculated magnetic force values with average rod velocities for several rods (Fig. 4a). Because all nanorods have a similar range of lengths, the nanorod force is primarily attributed to variations in rod diameters. Velocity versus force data (Fig. 4a) clearly demonstrates the pore-size effect:

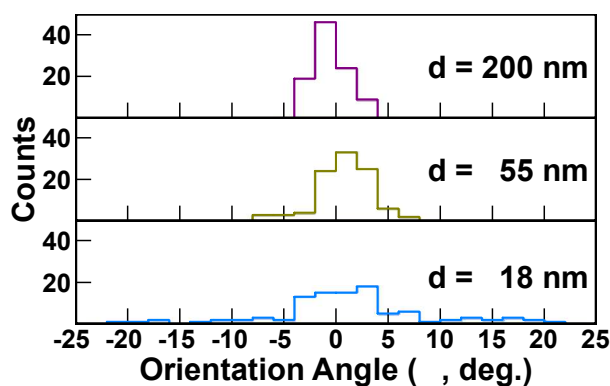


Figure 5: Nanorod orientation angles with respect to the magnetic field direction. Larger rods experience smaller translational diffusion. 200 nm, 55 nm, and 18 nm diameter rods experience maximum orientation angle deviations of  $\pm 4$ ,  $\pm 8$ , and  $\pm 22$  degrees, respectively.

smaller rods experiencing significantly less force move with significantly higher average velocities through the matrix. This demonstrates the limitations of using a purely Stokes-based drag force analysis of magnetophoresis through the extracellular matrix, which would predict larger velocities for larger particles experiencing larger forces. Previous magnetophoresis experiments performed on variously sized nanoparticles demonstrated differences in transport efficiency, noting that agglomerates of smaller particles moved more efficiently through ECM than agglomerates of large particles<sup>13</sup>. Our experiments build on these first demonstrations by applying single particle tracking for quantifying how force (particle size) impacts motion at the single particle level. Using this we directly observe the mechanisms by which smaller particles achieve enhanced motion through the ECM.

#### Apparent Viscosity

While taking a Stokes drag approach to calculating the force on a nanorod in Matrigel is inaccurate macroscopically, it can be useful for describing the average, apparent, local nanorod microenvironment. Each nanorod's gradient driven motion can be converted to an apparent viscosity using the incorrect assumption that Matrigel is a Newtonian solution, allowing us to compare apparent viscosities felt by rods of various diameters. We find that 55 nm and 200 nm diameter rods experience  $\eta_{\text{apparent}}$  values approximately two and four orders of magnitude larger than the  $\eta_{\text{apparent}}$  experienced by 18 nm rods, respectively (Fig. 4b). Apparent viscosity calculations on nanorods moving through Newtonian solutions will all yield the same apparent viscosity. Thus, we can attribute these variations in apparent viscosity entirely to diameter-dependent differences due to steric hindrance experienced by the nanorods as they move.

#### Orientation angle

In magnetophoresis through a Newtonian fluid, motion analysis is based on the Stokes-Einstein equation,  $F_{\text{magnetic}} = \beta \eta v$ , where  $\beta$  is the shape factor,  $\eta$  the viscosity, and  $v$  the particle velocity. Increased velocity can only be achieved by either (1) increasing the applied  $F_{\text{magnet}}$ , or (2) decreasing the medium viscosity. Indeed, it was previously suggested that applying AC magnetic fields (50 and 100 Hz) to particles during magnetophoresis induces local decreases in viscosity, thus enhancing particle transport velocities<sup>11</sup>. Because steric hindrance  $F_{\text{steric}}$  plays a major role in transport inhibition for

magnetophoresis through Matrigel, methods which operate to diminish the impacts of steric barriers, or avoid them altogether, will increase particle velocity. Translational diffusion is one such method of mediating the transport-diminishing impacts of steric barriers. Because translational diffusion allows a nanorod to tilt and thereby slide past a barrier in the ECM meshwork, it enhances a nanorod's chance of being pulled around a barrier by an applied field gradient. Narrow diameter nanorods not only have larger inherent translational diffusion coefficients, they also experience a smaller aligning force due to the applied magnetic field. To demonstrate variations in the translational diffusion coefficients of the nanorods in Matrigel we collect data on the orientation angle of various rods during their transit through the matrix. Fig. 5 shows this data in histogram form, demonstrating angular excursions away from the applied field angle are  $\pm 4$ ,  $\pm 8$ , and  $\pm 22$  degrees for 200, 55, 18 nm diameter nanorods, respectively. Thus, we propose that the translational diffusion force on narrow nanorods under a static magnetic force is one method serving to enhance transport. We suggest that the larger angular diffusion coefficients of small diameter nanorods allow these particles to occasionally evade steric barriers which permanently encumber larger diameter nanorods. This ability to bypass steric barriers and move through pores in the matrix is critical for small rods undergoing magnetophoresis. This observation suggests that active methods for increasing translational diffusion of nanorods may increase translational velocities in complex matrices. However, it is important to note that this feature cannot be conveyed to rods of any size. Clearly rods must have one dimension (specifically, the dimension at the translational front of the nanoparticle) sufficiently below the matrix mesh size for this translational mechanism to be relevant. This data is unique in the field of magnetophoresis, as most experiments are performed on spherical particles and do not include single particle tracking data.

#### Constant versus varying velocity motion

We demonstrate, for the first time, varying velocity motion for nanoparticles undergoing magnetophoresis in a biologically relevant polymer gel. The difficulties in traversing biological barriers such as the ECM have motivated various innovations aimed at enhancing nanoparticle transport, including attaching collagenase to particle surfaces<sup>14</sup>, engineering particle shape<sup>45</sup>, and applying AC magnetic fields<sup>11</sup>. Varying velocity motion, as demonstrated by the particle track shown in Fig. 6, points to increasing transport efficacy by a method of applying force which may not come to mind by only observing constant velocity motion or particle transport en masse. Small diameter nanorods experience large path deviations normal to the direction of the field gradient. The smaller diameter particles, being less magnetically confined, also exhibit significantly larger variation in orientation angle with respect to the magnetic field. Considering that this angular variation may aide the narrow particles in evading steric hindrances, the notion of applying either (1) forces normal to the intended direction of translation, or (2) torsional forces centered around the long axis of the nanorod, may assist in releasing nanoparticles from their local steric hindrances. Indeed, future experiments invoking single particle tracking may look to study how particle transport is impacted by applying transverse or torsional magnetic forces. The experiments performed by MacDonald et al. demonstrate that transport efficiency through a homogenous synthetic gel is significantly enhanced (30-fold enhancement was observed) by the application of a transverse AC field, and the reasoning used invokes changes in the local viscosity of the gel due to the oscillating motion of the particles. In a homogenous gel this serves as an excellent explanation of how AC fields applied transverse to the intended direction of motion may induce more rapid transport. Single particle tracking of magnetophoresis experiments

on nanorods in homogenous synthetic gels and inhomogenous biological gels may inform the field as to how AC fields operate to enhance transport through highly heterogeneous biomaterials. These findings suggest that, in designing a magnetic drug delivery system based on nanorods, applying forces normal to the intended direction of nanorod motion may aid in long range nanorod translation. The acceleration-deceleration motion observed for small rods may also suggest that balancing force application and free diffusion may lead to faster translational velocities, as durations of free diffusion may ensure that a particle is not being continually pulled into a mesh of tissue too dense to effectively move through.

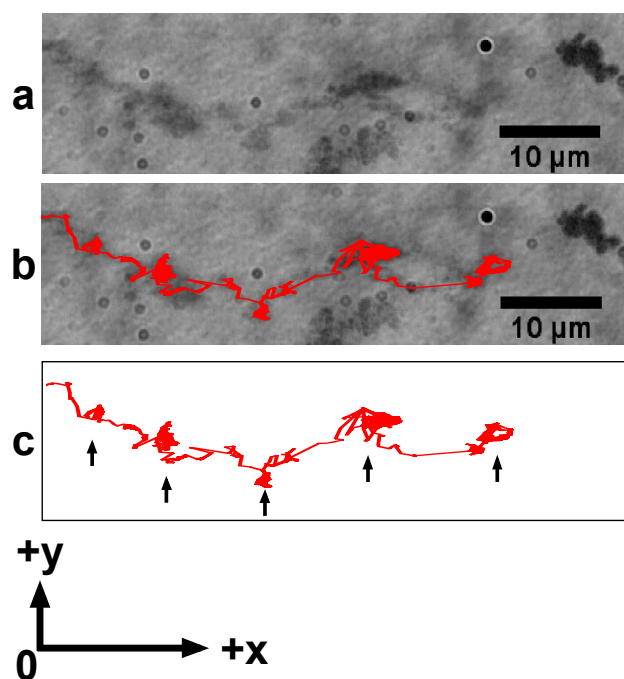


Figure 6: Acceleration-deceleration motion observed for 18 nm diameter nanorods during magnetophoresis. (a) Minimum intensity projections of nanorods moving through ECM (1 frame per second) can be tracked (b) and demonstrates locations of significant steric hindrance (c, arrows). Particle motion, and direction of increasing magnetic gradient, is in the +x direction. Significant motion in the +/-y directions, as well as motion in the -x direction, elucidates the complexity of magnetophoretic transport for small diameter nanorods in dense polymer networks.

#### Drug delivery figures of merit

While quantification of nanoparticle magnetophoresis at the single particle level informs our understanding of transport dynamics through complex biological environments, its medical relevance is only fully realized by applying figures of merit that indicate if the variations in average velocity will actually result in more efficient delivery of pharmaceutical payloads. Currently nanoparticle drug carriers transport their cargo by either volume loading (the drug is encapsulated within the volume of the particle) or surface loading (the drug is attached to the surface of the particle). Normalizing average velocities per particle by the specific particle's volume or surface area creates two figures of merit to address each type of cargo carrying method. Fig. 7 demonstrates these two figures of merit. Performing this simple normalization indicates that, in our experiments, 18 nm rods are slightly less efficient at moving payloads via volume loading (7a), and approximately equivalently

efficient at moving payloads via surface loading (7b). Using these and similar figures of merit will be important in optimizing future particles with respect to size, shape, and transport velocities in biological materials. This result highlights the notion that magnetophoretic velocity is only one component of a particle's overall usefulness in delivering therapeutic payloads, and should be incorporated into figure of merit calculations with take into account an overall efficacy of delivery.

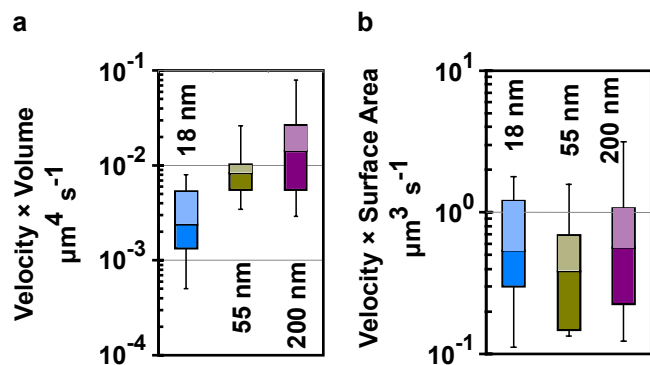


Figure 7: Figures of merit based on (a) volume and (b) surface area loading of a relevant drug or therapeutic molecule. Normalizing particle velocity through multiplying velocity by volume or surface area provides a more applicable understanding of how particle size and velocity through ECM should be assessed for delivering molecules efficiently.

## Conclusions

These experiments are the first demonstrations of single particle magnetophoresis through polymer matrices. They offer insight as to how varying particle sizes and forces impact particle transport through complex biological matrices at the single particle level. It has been long accepted that size and shape matter in drug delivery for processes such as EPR retention, circulation time<sup>46</sup>, passage through the blood brain barrier, diffusion through ECM<sup>47</sup>, and myriad other processes<sup>48</sup>. Here we demonstrate how magnetophoresis through the ECM varies for particles of different sizes. In addition to demonstrating fits-and-starts styled motion, we propose the notion of angular diffusion playing a significant role in allowing narrow nanorods to escape from protein dense ECM regions which provide large steric force hindrance. This notion raises the question of whether too much force may actually serve to diminish transport velocities by significantly suppressing angular diffusion.

The experiments described herein open up new understandings on magnetophoretic motion of particles through complex networks of biopolymers. We observe significantly varying velocities, and functionally different modes of translation, for nanorods of varying diameters. However, despite these large variations in velocity, we observe surprisingly small differences in the figures of merit that quantify payload delivery. Our quantification of how individual particle velocities translate to volume or surface loaded payload delivery may provide useful information for the future design of particles designed to translate long distances (hundreds of micrometers or more) through biopolymers. While we have used Matrigel to test nanoparticle transport, the parameter space for testing is large. Drug delivery through mucus, serum, and biomembranes could all be studied in a similar manner.

Additionally, our experiments probe a small fraction of the particle shape parameter space. Researchers have shown that particle

shape plays an important role in how biological entities interface with micro- and nanoscale particles<sup>46,49</sup>. New techniques have been developed for imparting exquisite control over particle shape<sup>50,51</sup>. Future experiments exploring how exotically shaped particles move through biopolymers may elucidate shape-dependent transport mechanisms which engineers and pharmaceutical scientists can exploit to create more effective drug delivery vehicles.

## Acknowledgements

The authors would like to acknowledge the help of Wallace Ambrose of the UNC Chapel Hill Analytical and Nanofabrication Laboratory for help in preparing the Matrigel samples for SEM imaging. LOM acknowledges the Ross and Charlotte Johnson Family Dissertation Fellowship, graciously provided through the UNC Graduate School, for partially funding this research. This research was also supported by NIH #P41EB002025. The authors have no other relevant affiliations or financial involvement with any organization or entity with a financial interest in or financial conflict with the subject matter or materials discussed in the manuscript apart from those disclosed.

## Notes

<sup>a</sup> Curriculum in Applied Sciences and Engineering, University of North Carolina, Chapel Hill, NC 27599 USA. \*Email: Lamar.Mair@gmail.com

<sup>b</sup> Department of Physics and Astronomy, University of North Carolina, Chapel Hill, NC 27599 USA.

<sup>c</sup> Currently at Weinberg Medical Physics, Bethesda, MD 20814 USA.

Electronic Supplementary Information (ESI) available: [details of any supplementary information available should be included here]. See DOI: 10.1039/b000000x/

## References

- R. K. Jain and T. Stylianopoulos, *Nat. Rev. Clin. Onc.*, 2010, **7**, 653–664.
- J. H. Grossman and S. E. McNeil, *Phys. Today*, 2012, **65**, 38.
- S. H. Jang, M. G. Wientjes, D. Lu, and J. L. S. Au, *Pharm. Res.*, 2003, **20**, 1337–1350.
- A. I. Minchinton and I. F. Tannock, *Nat. Rev. Cancer*, 2006, **6**, 583–592.
- O. Trédan, C. M. Galmarini, K. Patel, and I. F. Tannock, *J. Natl. Cancer I.*, 2007, **99**, 1441–1454.
- H. Holback and Y. Yeo, *Pharm. Res.*, 2011, **28**, 1819–1830.
- D. L. Holligan, G. T. Gillies, and J. P. Dailey, *Nanotechnology*, 2003, **14**, 661–666.
- O. Rotariu, L. E. Udrea, N. J. C. Strachan, and V. Bădescu, *J. Optoelectron. Adv. M.*, 2007, **9**, 942–945.
- M. Salloum, R. H. Ma, D. Weeks, and L. Zhu, *Int. J. Hyperther.*, 2008, **24**, 337–345.
- S. Basak, D. Brogan, H. Dietrich, R. Ritter, R. G. Dacey, and P. Biswas, *Int. J. Nanomed.*, 2009, **4**, 9–26.

11. C. MacDonald, G. Friedman, J. Alamia, K. Barbee, and B. Polyak, *Nanomedicine (Lond.)*, 2010, **5**, 65–76.
12. V. S. Kalambur, B. Han, B. E. Hammer, T. W. Shield, and J. C. Bischof, *Nanotechnology*, 2005, **16**, 1221.
13. S. J. Kuhn, D. E. Hallahan, and T. D. Giorgio, *Ann. Biomed. Eng.*, 2006, **34**, 51–58.
14. S. J. Kuhn, S. K. Finch, D. E. Hallahan, and T. D. Giorgio, *Nano Lett.*, 2006, **6**, 306–312.
15. J. A. Cribb, T. D. Meehan, S. M. Shah, K. Skinner, and R. Superfine, *Ann. Biomed. Eng.*, 2010, **38**, 3311–3322.
16. P. Ruenaroengsak, J. M. Cook, and A. T. Florence, *J. Control. Release*, 2010, **141**, 265–276.
17. S. K. Hobbs, W. L. Monsky, F. Yuan, W. G. Roberts, L. Griffith, V. P. Torchilin, and R. K. Jain, *Proc. Natl. Acad. Sci. USA*, 1998, **95**, 4607–4612.
18. S. K. Lai, D. E. O'Hanlon, S. Harrold, S. T. Man, Y.-Y. Wang, R. Cone, and J. Hanes, *Proc. Natl. Acad. Sci. USA*, 2007, **104**, 1482–1487.
19. O. Lieleg, R. M. Baumgärtel, and A. R. Bausch, *Biophys. J.*, 2009, **97**, 1569–1577.
20. O. Lieleg, I. Vladescu, and K. Ribbeck, *Biophys. J.*, 2010, **98**, 1782–1789.
21. J. Dobson, *Nanomedicine (Lond.)*, 2006, **1**, 31–37.
22. N. S. Barakat, *Nanomedicine (Lond.)*, 2009, **4**, 799–812.
23. E. Gultepe, F. J. Reynoso, A. Jhaveri, P. Kulkarni, D. Nagesha, C. Ferris, M. Harisinghani, R. B. Campbell, and S. Sridhar, *Nanomedicine (Lond.)*, 2010, **5**, 1173–1182.
24. R. Sensenig, Y. Sapir, C. Macdonald, S. Cohen, and B. Polyak, *Nanomedicine (Lond.)*, 2012, **7**, 1425–1442.
25. A. S. Lubbe, C. Bergemann, J. Brock, and D. G. McClure, *J. Magn. Mater.*, 1999, **194**, 149–155.
26. P. D. Yurchenco and H. Furthmayr, *Biochemistry*, 1984, **23**, 1839–1850.
27. P. D. Yurchenco and G. C. Ruben, *J. Cell. Biol.*, 1987, **105**, 2559–2568.
28. P. D. Yurchenco and G. C. Ruben, *Am. J. Pathol.*, 1988, **132**, 278–291.
29. I. Hunter, J. Engel, and B. Chemistry, *FASEB J.*, 1990, **4**, 148–160.
30. J. Kirch, A. Schneider, B. Abou, A. Hopf, U. F. Schaefer, M. Schneider, C. Schall, C. Wagner, and C.-M. Lehr, *Proc. Natl. Acad. Sci. U. S. A.*, 2012, **109**, 18355–60.
31. T. Stylianopoulos, M.-Z. Poh, N. Insin, M. G. Bawendi, D. Fukumura, L. L. Munn, and R. K. Jain, *Biophys. J.*, 2010, **99**, 1342–1349.
32. R. M. Penner and C. R. Martin, *Anal. Chem.*, 1987, **59**, 2625–2630.
33. C. R. Martin, *Science (80- )*, 1994, **266**, 1961–1966.
34. A. Fert and L. Piraux, *J. Magn. Magn. Mater.*, 1999, **200**, 338–358.
35. Z. Yang, J. A. Galloway, and H. Yu, *Langmuir*, 1999, **15**, 8405–8411.
36. N. D. Winblade, I. D. Nikolic, A. S. Hoffman, and J. A. Hubbell, *Biomacromolecules*, 2000, **1**, 523–533.
37. J. V. Jokerst, T. Lobovkina, R. N. Zare, and S. S. Gambhir, *Nanomedicine (Lond.)*, 2011, **6**, 715–728.
38. Y. Zhang, N. Kohler, and M. Zhang, *Biomaterials*, 2002, **23**, 1553–1561.
39. H. K. Kleinman, M. L. Mcgarvey, L. A. Liotta, P. G. Robey, K. Tryggvason, and G. R. Martin, *Biochemistry*, 1982, **21**, 6188–6193.
40. R. M. Taylor, *online at [http://cisimm.cs.unc.edu/downloads/?dl\\_cat=3](http://cisimm.cs.unc.edu/downloads/?dl_cat=3)*, 2009.
41. J. Lim, C. Lanni, E. R. Evarts, F. Lanni, R. D. Tilton, and S. A. Majetich, *ACS Nano*, 2010.
42. L. Mair, K. Ford, R. Alam, R. Kole, and M. Fisher, *J. Biomed. Nanotechnol.*, 2009, **5**.
43. A. K. Andriola Silva, R. Di Corato, F. Gazeau, T. Pellegrino, and C. Wilhelm, *Nanomedicine (Lond.)*, 2012, **7**, 1713–1727.
44. J. A. Osborn, *Phys. Rev.*, 1945, **67**, 351–357.
45. S. Mitragotri and J. Lahann, *Nat. Mater.*, 2009, **8**, 15–23.
46. Y. A. N. Geng, P. Dalhaimer, S. Cai, R. Tsai, M. Tewari, T. Minko, and D. E. Discher, *Nat. Nanotechnol.*, 2007, **2**, 249–255.
47. G. Alexandrakis, E. B. Brown, R. T. Tong, T. D. McKee, R. B. Campbell, Y. Boucher, and R. K. Jain, *Nat. Med.*, 2004, **10**, 203–207.
48. S. Mitragotri, *Pharm. Res.*, 2009, **26**, 232–234.
49. S. E. A. Gratton, P. A. Ropp, P. D. Pohlhaus, J. C. Luft, V. J. Madden, M. E. Napier, and J. M. DeSimone, *Proc. Natl. Acad. Sci. USA*, 2008, **105**, 11613–8.
50. L. E. Euliss, J. A. DuPont, S. Gratton, and J. DeSimone, *Chem. Soc. Rev.*, 2006, **35**, 1095–104.
51. J. A. Champion, Y. K. Katare, and S. Mitragotri, *Proc. Natl. Acad. Sci. USA*, 2007, **104**, 11901–4.